Commun. Comput. Phys.
doi: 10.4208/cicp.OA-2017-0003

Vol. **22**, No. 5, pp. 1413-1438
November 2017

Topology Optimization of Capillary, Two-Phase Flow Problems

Yongbo Deng[1,*], Zhenyu Liu[2] and Yihui Wu[1]

[1] *State Key Laboratory of Applied Optics, Changchun Institute of Optics, Fine Mechanics and Physics (CIOMP), Chinese Academy of Sciences, Changchun 130033, China.*
[2] *Changchun Institute of Optics, Fine Mechanics and Physics (CIOMP), Chinese Academy of Sciences, Changchun 130033, China.*

Received 5 January 2017; Accepted (in revised version) 10 April 2017

Abstract. This paper presents topology optimization of capillary, the typical two-phase flow with immiscible fluids, where the level set method and diffuse-interface model are combined to implement the proposed method. The two-phase flow is described by the diffuse-interface model with essential no slip condition imposed on the wall, where the singularity at the contact line is regularized by the molecular diffusion at the interface between two immiscible fluids. The level set method is utilized to express the fluid and solid phases in the flows and the wall energy at the implicit fluid-solid interface. Based on the variational procedure for the total free energy of two-phase flow, the Cahn-Hilliard equations for the diffuse-interface model are modified for the two-phase flow with implicit boundary expressed by the level set method. Then the topology optimization problem for the two-phase flow is constructed for the cost functional with general formulation. The sensitivity analysis is implemented by using the continuous adjoint method. The level set function is evolved by solving the Hamilton-Jacobian equation, and numerical test is carried out for capillary to demonstrate the robustness of the proposed topology optimization method. It is straightforward to extend this proposed method into the other two-phase flows with two immiscible fluids.

AMS subject classifications: 76D55, 76D45, 76T10, 65K10, 65M60
Key words: Capillary, two-phase flow, topology optimization, diffuse-interface model, level set method.

1 Introduction

The topology optimization method for the fluid flow was pioneered by Steven et al. [1] and Borrvall et al. [2]. Topology optimization was first used to design stiffness and com-

*Corresponding author. *Email addresses:* dengyb@ciomp.ac.cn (Y. Deng), liuzy@ciomp.ac.cn (Z. Liu), yihuiwu@ciomp.ac.cn (Y. Wu)

 ©2017 Global-Science Press

https://doi.org/10.4208/cicp.OA-2017-0003 Published online by Cambridge University Press

pliance mechanisms [3–6], and it has been extended to multiple physical problems, such as acoustic, electromagnetic, fluidic, optical and thermal problems [2,7–12]. Several approaches, such as the evolutionary techniques [1,13,14], homogenization method [3,15], density method (solid isotropic material with penalization) [7,16–19], level set method [20–26] and phase field method [27–34], have been developed for the implementation of topology optimization. Topology optimization of fluid flows has mainly focused on the single phase flows [18,19,22,26,35–38], and the multi-component flows without surface tension [39,40]. The two-phase flow of immiscible fluids with surface tension plays a fundamental role in many natural and industrial phenomena. Examples can be found in the studies of capillarity, low-gravity fluid flow, hydrodynamic stability, surfactant behavior, cavitation, and droplet dynamics. For the academic and engineering requirement, this paper focuses on developing the topology optimization method for the two-phase flows of immiscible fluids.

At the interface of two immiscible fluids, the cohesive forces within the fluid and adhesive forces between the fluid and its surroundings give rise to the surface tension [41]. Due to the surface tension, the complexity on dealing with moving interfaces in two phase flows are encountered from the mathematical modeling and numerical algorithmic points of view. There are many approaches to characterize moving interfaces. The two main approaches are interface tracking and interface capturing methods. In interface tracking methods (e.g. volume-of-fluid [42], front-tracking [43], and immersed boundary [44, 45]), Lagrangian particles are used to track the interfaces, and these particles are advected by the velocity field, where the difficulties on capturing the topological changes of the moving interface are encountered. In the interface capturing methods (e.g. the level set method [46–50] and diffuse interface method [51–54]), the interface is implicitly captured by a contour of a particular scalar function, and the topological changes of the interface can be flexibly treated. Therefore, the robust interface capturing methods are more popularly used in the simulation of two-phase flows, compared to the interface tracking methods.

In topology optimization of fluid flows, the solid phase is approximated using the fluid velocity penalization method, which is implemented by adding the artificial Darcy forces into the Navier-Stokes equations [2]. Based on the fluid velocity penalization method, the no-slip boundary condition is achieved at the implicit interface between the fluid and solid phases. In the simulation of two-phase flows, the stress singularity and infinite dissipation problem are encountered near the three-phase contact line of the two-phase flow, when the no-slip boundary condition is imposed on the walls of the two-phase flow directly [55,56]. The singularity can be solved using the slip model [55] or diffuse interface method [56]. In the slip model, the slip boundary condition with the slip velocity proportional to the tangential stress is imposed on the walls. This is incompatible with the fluid velocity penalization method. On the other hand, the diffuse interface method solves the singularity and evolves the interface and three-phase contact line based on the molecular diffusion driven by chemical potential, with the no slip condition imposed on the wall. Therefore, the diffuse interface method is the reasonable choice to

https://doi.org/10.4208/cicp.OA-2017-0003 Published online by Cambridge University Press

describe the two-phase flow in the corresponding topology optimization problem with no slip boundary condition at the fluid-solid interface with the solid phase approximated using the fluid velocity penalization method.

In the diffuse interface method for two-phase flow, the phase field is used to distinguish the two immiscible fluids, and the evolution of the phase field is governed by the Cahn-Hilliard equations, which is obtained based on the surface free energy minimum principle [57]. In topology optimization, the wall energy (i.e. the surface free energy at the fluid-solid interface) of the implicit solid-fluid boundary of the two-phase flow is one part of the total surface free energy. In order to consider the wall energy of the implicit boundary, the implicit boundary is required to have an exact mathematical expression on its normal vector and curvature. Therefore, the level set method, which can exactly satisfy this requirement [20–23, 35, 49, 50, 58], is adopted to implement the topology optimization of two-phase flows.

It is noticed that the phase field in this paper is used to describe the two immiscible fluids in the dynamics of two-phase flow, and it is not the case in phase field method-based topology optimization; instead, the level set method is utilized to implement the topology optimization of two-phase flow, where the solid phase is approximated by the fluid velocity penalization method. The remainder of this paper is recognized as follows: the level set method based implicit expression of two-phase flow and the corresponding governing equations are introduced in Section 2; the topology optimization problem is constructed and the corresponding sensitivity analysis is performed in Section 3; the numerical implementation and numerical examples are presented in Section 4; and the paper is concluded in Section 5. In the following, all the mathematical descriptions are implemented in the Cartesian coordinate system.

2 Level set method based implicit expression of two-phase flow and the corresponding governing equations

2.1 Level set method based implicit expression of two-phase flow

Based on the level set method, the solid and fluid phases in the two-phase flow can be distinguished implicitly using the sign of the level set function, which is usually expressed to be a signed distance function defined in the optimization domain [49]. Then, the solid-fluid boundary can be represented by the zero level set of the level set function. The implicit expression used in this paper is presented as follows (Fig. 1)

$$\begin{cases} \varphi(\mathbf{x}) < 0, & \forall \mathbf{x} \in \Omega_s, \\ \varphi(\mathbf{x}) > 0, & \forall \mathbf{x} \in \Omega_l, \\ \varphi(\mathbf{x}) = 0, & \forall \mathbf{x} \in \Gamma, \end{cases} \tag{2.1}$$

where φ is the level set function satisfying $|\nabla\varphi| = 1$ and the operator $|\cdot|$ represents the norm of a vector; Ω_s, Ω_l and Γ are the solid, fluid and implicit boundary, respectively; Ω_s

https://doi.org/10.4208/cicp.OA-2017-0003 Published online by Cambridge University Press

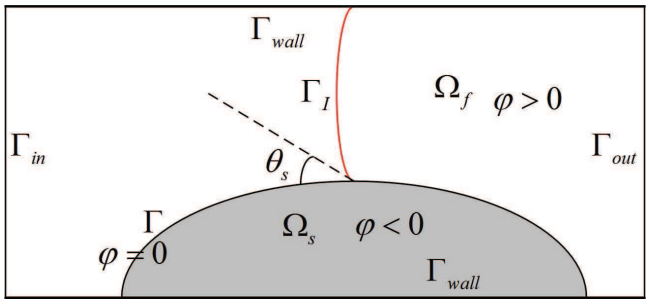


Figure 1: Schematic for the level set based implicit expression of the two-phase flow. Ω_s is the solid phase; Ω_f is the fluid phase; Γ is the implicit solid-fluid boundary; Γ_I is the interface between the two immiscible fluids; θ_s is the contact angle formed by the tangents of the solid surface and immiscible interface; φ is the level set function; Γ_{in}, Γ_{wall} and Γ_{out} are the inlet, wall and outlet boundaries of the optimization domain, respectively.

and Ω_l are open, and they satisfy $\overline{\Omega}_s \cup \overline{\Omega}_l = \overline{\Omega}$ (Ω is the optimization domain).

Based on the implicit expression demonstrated in Eq. (2.1), the solid phase is approximated by the fluid velocity penalization method, i.e. adding the artificial Darcy force into the body force term of the Navier-Stokes equations [2], with the artificial Darcy force expressed as

$$\mathbf{f}_r = -\rho\alpha(\varphi)\mathbf{u}, \tag{2.2}$$

where ρ is the fluid density; $\mathbf{u}$ is the fluid velocity; $\alpha(\varphi)$ is the impermeability, and it is interpolated by the level set function

$$\alpha(\varphi) = \alpha_s + (\alpha_f - \alpha_s) H(\varphi), \tag{2.3}$$

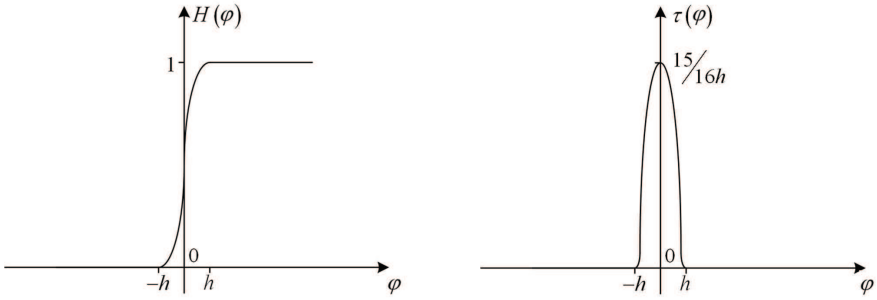
with α_f and α_s representing the impermeability of the fluid and artificial solid phases, respectively. Theoretically, α_f and α_s are respectively equal to zero and infinity. However, α_s should be chosen to be a high but finite positive number to simultaneously approximate the solid and ensure the numerical stability. In Eq. (2.3), $H(\varphi)$ is the Heaviside function expressed to be

$$H(\varphi) = \begin{cases} 1, & \varphi \geq 0, \\ 0, & \varphi < 0. \end{cases} \tag{2.4}$$

The derivative of the Heaviside function to φ is the Dirac function $\tau(\varphi)$. In most cases, the Heaviside function and the Dirac function need to be regularized from the numerical implementation point of view. In this paper, $H(\varphi)$ and $\tau(\varphi)$ are approximated by the smoothed Heaviside function and Dirac function [59]

$$H(\varphi) = \begin{cases} 0, & \varphi \leq -h, \\ \dfrac{1}{2} + \dfrac{15\varphi}{16h} - \dfrac{5\varphi^3}{8h^3} + \dfrac{3\varphi^5}{16h^5}, & -h < \varphi \leq h, \\ 1, & \varphi > h, \end{cases} \tag{2.5}$$

https://doi.org/10.4208/cicp.OA-2017-0003 Published online by Cambridge University Press



(a) Heaviside function (b) Dirac function

Figure 2: Schematic for the regularized Heaviside function and Dirac function of the level set function, where h is the support size.

$$\tau(\varphi)=\begin{cases}\dfrac{15}{16h}\left(1-\dfrac{\varphi^2}{h^2}\right)^2, & |\varphi|\le h,\\ 0, & |\varphi|>h,\end{cases} \tag{2.6}$$

where h is the support size (Fig. 2).

2.2 Governing equations

The two-phase flow is described by the diffuse-interface model to regularize the singularity at the contact line, with no slip boundary condition on the wall. Then the fluid velocity penalization method is utilized to implicitly express the no slip boundary condition at the interface between solid and fluid phases. In the diffuse-interface model, the phase field is defined to represent and evolve the two immiscible fluids in the two-phase flow. And the evolution of the phase field is governed by the Cahn-Hilliard equations [57, 60], which are derived based on the surface free energy minimum principle [57]. In topology optimization, the interface between solid and fluid phases is expressed implicitly. This causes the change of the expression of the total free energy. Therefore, the Cahn-Hilliard equations need to be modified for the flow domain implicitly expressed by the level set method. According to [57], the total free energy of the two-phase flow in the optimization domain shown in Fig. 1 can be written as follows by introducing the phase field variable ϕ satisfying $\phi=\pm1$ in the two-fluid bulks and $\phi=0$ at the fluid-fluid interface

$$\begin{aligned}\mathcal{F}&=\int_\Omega f_m(\phi,\nabla\phi)\,\mathrm{d}\Omega+\int_\Gamma f_w(\phi)\,\mathrm{d}\Gamma+\int_{\Gamma_{wall}} f_w(\phi)\,\mathrm{d}\Gamma\\&=\int_\Omega\left[f_m(\phi,\nabla\phi)+f_w(\phi)\tau(\varphi)|\nabla\varphi|\right]\mathrm{d}\Omega+\int_{\Gamma_{wall}} f_w(\phi)\,\mathrm{d}\Gamma,\end{aligned} \tag{2.7}$$

where $f_m(\phi,\nabla\phi)$ and $f_w(\phi)$ are respectively the fluid-fluid mixing energy in the two immiscible fluids [57] and wall energy at the fluid-solid interface Γ_{wall} [56, 61]. Based on

https://doi.org/10.4208/cicp.OA-2017-0003 Published online by Cambridge University Press

the implicit expression of the two-phase flow described in Section 2.1, the mixing energy and wall energy are modified to be

$$f_m(\phi,\nabla\phi)=\frac{\lambda(\varphi)}{2}|\nabla\phi|^2+\frac{\lambda(\varphi)}{4\epsilon^2}\left(\phi^2-1\right)^2, \tag{2.8a}$$

$$f_w(\phi)=\begin{cases} -\sigma_0\dfrac{\phi\left(3-\phi^2\right)}{4}\cos\theta_s+\dfrac{\sigma_{w1}+\sigma_{w2}}{2}, & \text{on } \Gamma, \\ -\sigma(\varphi)\dfrac{\phi\left(3-\phi^2\right)}{4}\cos\theta_s+\dfrac{\sigma_{w1}+\sigma_{w2}}{2}H(\varphi), & \text{on } \Gamma_{wall}, \end{cases} \tag{2.8b}$$

where $\lambda(\varphi)$ is the mixing energy density interpolated by the level set function; ϵ is the capillary width; θ_s is the contact angle formed by the tangents of the solid surface and immiscible interface; σ_0 is the surface tension at the interface between the two immiscible fluids; σ_{w1} and σ_{w2} are the fluid-solid interfacial tension for the two fluids, respectively; in equilibrium, the fluid-fluid interfacial tension is defined by the mixing energy density $\lambda(\varphi)$ and capillary width ϵ

$$\sigma=\frac{2\sqrt{2}}{3}\frac{\lambda(\varphi)}{\epsilon}. \tag{2.9}$$

In principle, the interpolated mixing energy density $\lambda(\varphi)$ should keep its value in the fluid phase Ω_f and vanish to be zero in the solid phase Ω_s. To ensure the numerical stability, $\lambda(\varphi)$ is set to be a nonzero but small enough positive value. Therefore, the interpolation of the mixing energy density is set to be

$$\lambda(\varphi)=\lambda_s+\left(\lambda_f-\lambda_s\right)H(\varphi), \tag{2.10}$$

where λ_f and λ_s are the mixing energy density for the fluid and approximated solid phases, respectively. According to Eq. (2.10), one can see that σ_0 satisfies $\sigma_0=\frac{2\sqrt{2}}{3}\frac{\lambda_f}{\epsilon}$.

Based on the variational procedure introduced in [55,56], the chemical potential and the boundary condition for the phase field can be obtained as

$$\begin{aligned} &\psi=\frac{\delta\mathcal{F}}{\delta\phi}=\left[-\nabla\cdot(\lambda(\varphi)\nabla\phi)+\frac{\lambda(\varphi)}{\epsilon^2}\phi\left(\phi^2-1\right)\right]-\frac{3}{4}\sigma_0\left(1-\phi^2\right)\cos\theta_s\tau(\varphi)|\nabla\varphi|, \quad \text{in } \Omega, \\ &\lambda(\varphi)\mathbf{n}\cdot\nabla\phi-\frac{3}{4}\sigma(\varphi)\left(1-\phi^2\right)\cos\theta_s=0, \quad \text{on } \Gamma_{wall}, \end{aligned} \tag{2.11}$$

and the body force that is the diffuse-interface equivalent of the interfacial tension [62]

$$\mathbf{f}_s=H(\varphi)\psi\nabla\phi \tag{2.12}$$

is added to the Navier-Stokes equations, where $H(\varphi)$ is used to penalize the interfacial tension and avoid the fluid flow driven by the interfacial tension in the artificial solid phase with $\varphi<0$ [36]. The evolution of the phase filed variable is governed by the following equation [63]

$$\frac{\partial\phi}{\partial t}+\mathbf{u}\cdot\nabla\phi=\nabla\cdot[M(\varphi)\nabla\psi], \tag{2.13}$$

https://doi.org/10.4208/cicp.OA-2017-0003 Published online by Cambridge University Press

where $M(\varphi)>0$ is the mobility or Onsager coefficient. Eq. (2.13) models the creation, evolution, and dissolution of diffusively controlled phase-field interfaces. In the implicitly expressed two-phase flow, the mobility keeps its value in the fluid phase and is equal to infinity in the solid phase theoretically. Therefore, the mobility is also interpolated by the level set function. Being similar with the impermeability, the mobility is also assigned to be a high but finite value in the approximated solid phase, to ensure the numerical stability. Then the interpolation of the mobility is set to be

$$M(\varphi)=M_s+\left(M_f-M_s\right)H(\varphi), \tag{2.14}$$

where M_f and M_s are the mobility for the fluid and approximated solid phases, respectively.

Based on the above procedure, the governing equations for the two-phase flow implicitly expressed using the level set method are:

Navier-Stokes equations:

$$\begin{cases}\rho\left(\dfrac{\partial\mathbf{u}}{\partial t}+\mathbf{u}\cdot\nabla\mathbf{u}\right)=\nabla\cdot\left[-p\mathbb{I}+\eta\left(\nabla\mathbf{u}+\nabla\mathbf{u}^{\mathrm{T}}\right)\right]+H(\varphi)\psi\nabla\phi-\rho\alpha(\varphi)\mathbf{u},\\ -\nabla\cdot\mathbf{u}=0;\end{cases} \tag{2.15a}$$

Cahn-Hilliard equations:

$$\begin{cases}\dfrac{\partial\phi}{\partial t}+\mathbf{u}\cdot\nabla\phi=\nabla\cdot[M(\varphi)\nabla\psi],\\ \psi=\left[-\nabla\cdot(\lambda(\varphi)\nabla\phi)+\dfrac{\lambda(\varphi)}{\epsilon^2}\phi\left(\phi^2-1\right)\right]-\dfrac{3}{4}\sigma_0\left(1-\phi^2\right)\cos\theta_s\tau(\varphi)|\nabla\varphi|,\end{cases} \tag{2.15b}$$

where ρ is the fluid density; η is the dynamic viscosity of fluid; p is the pressure; $\mathbb{I}$ is the unit tensor. In Eq. (2.15), the density and dynamic viscosity are functions of the phase field variable

$$\begin{aligned}\rho(\phi)&=\rho_2+(\rho_1-\rho_2)H(\phi),\\ \eta(\phi)&=\eta_2+(\eta_1-\eta_2)H(\phi),\end{aligned} \tag{2.16}$$

where ρ_1 and ρ_2 are the density of the two fluids, respectively; η_1 and η_2 are the dynamic viscosity of the two fluids, respectively; $H(\phi)$ is the Heaviside function of the phase field variable ϕ; $H(\phi)$ and its derivative $\tau(\phi)$ are smoothed similar to Eqs. (2.5) and (2.6). The initial condition and boundary conditions for the governing equations (2.15) are listed as follows: initial condition

$$\begin{aligned}\mathbf{u}(t=0)&=\mathbf{u}_0,\\ \phi(t=0)&=\phi_0,\end{aligned} \tag{2.17}$$

https://doi.org/10.4208/cicp.OA-2017-0003 Published online by Cambridge University Press

with initial interface represented by $\phi_0=0$; boundary condition at the inlet

$$\begin{aligned}&\left[-p\mathbb{I}+\eta\left(\nabla\mathbf{u}+\nabla\mathbf{u}^{\mathrm{T}}\right)\right]\cdot\mathbf{n}=\mathbf{0},\\&\mathbf{n}\cdot[M(\varphi)\nabla\psi]=0,\\&\phi=\phi_{in};\end{aligned}\tag{2.18}$$

boundary condition at the wall

$$\begin{aligned}&\mathbf{u}=\mathbf{0},\\&\mathbf{n}\cdot[M(\varphi)\nabla\psi]=0,\\&\lambda(\varphi)\mathbf{n}\cdot\nabla\phi-\frac{3}{4}\sigma(\varphi)\left(1-\phi^2\right)\cos\theta_s=0;\end{aligned}\tag{2.19}$$

and boundary condition at the outlet

$$\begin{aligned}&\left[-p\mathbb{I}+\eta\left(\nabla\mathbf{u}+\nabla\mathbf{u}^{\mathrm{T}}\right)\right]\cdot\mathbf{n}=\mathbf{0},\\&\mathbf{n}\cdot[M(\varphi)\nabla\psi]=0,\\&\lambda(\varphi)\mathbf{n}\cdot\nabla\phi=0,\end{aligned}\tag{2.20}$$

where the inlet and outlet boundaries are set to be open type and the wall is set to be no slip type.

3 Topology optimization problem and sensitivity analysis

3.1 Topology optimization problem

Based on the level set method based implicit expression of the two-phase flow and the modified governing equations introduced in Section 2, the topology optimization problem for the two-phase flow can be constructed as:

Maximize or minimize $J(\mathbf{u},p,\psi,\phi;\varphi)$, subject to

$$\begin{cases}\rho\left(\dfrac{\partial\mathbf{u}}{\partial t}+\mathbf{u}\cdot\nabla\mathbf{u}\right)=\nabla\cdot\left[-p\mathbb{I}+\eta\left(\nabla\mathbf{u}+\nabla\mathbf{u}^{\mathrm{T}}\right)\right]+H(\varphi)\psi\nabla\phi-\rho\alpha(\varphi)\mathbf{u}, & \text{in } (0,T)\times\Omega,\\ -\nabla\cdot\mathbf{u}=0, & \text{in } (0,T)\times\Omega,\\ \dfrac{\partial\phi}{\partial t}+\mathbf{u}\cdot\nabla\phi=\nabla\cdot[M(\varphi)\nabla\psi], & \text{in } (0,T)\times\Omega,\\ \psi=-\nabla\cdot[\lambda(\varphi)\nabla\phi]+\dfrac{\lambda(\varphi)}{\epsilon^2}\phi\left(\phi^2-1\right)-\dfrac{3}{4}\sigma_0\left(1-\phi^2\right)\cos\theta_s\tau(\varphi)|\nabla\varphi|, & \text{in } (0,T)\times\Omega,\\ \displaystyle\int_\Omega H(\varphi)\,\mathrm{d}\Omega=V^*V_0,\end{cases}\tag{3.1}$$

https://doi.org/10.4208/cicp.OA-2017-0003 Published online by Cambridge University Press

where the optimization problem is regularized by a volume constraint; V^* is the volume fraction of the fluid phase; V_0 is the volume of the optimization domain; $(0,T)$ is the considered time interval. In this optimization problem, the level set function φ is the design variable, which will be iteratively evolved for the derivation of the optimal structural topology used to control the two-phase flow. The general optimization objective functionals, which include both the domain and boundary integrations about the unknowns of the governing equations, are chosen to be

$$J(\mathbf{u},p,\psi,\phi)=\int_0^T\int_\Omega \omega_1 A(\mathbf{u},\nabla\mathbf{u},p,\psi,\nabla\psi,\phi,\nabla\phi;H(\varphi))\,\mathrm{d}\Omega\mathrm{d}t + \int_0^T\int_{\partial\Omega}\omega_2 B(\mathbf{u},p,\psi,\phi;H(\varphi))\,\mathrm{d}\Gamma\mathrm{d}t+\int_0^T\int_\Gamma \omega_3 C(\mathbf{u},p,\psi,\phi)\,\mathrm{d}\Gamma\mathrm{d}t, \tag{3.2}$$

where A, B and C are respectively the integral functional defined on the optimization domain, domain boundary and zero level set; ω_1, ω_2 and ω_3, satisfying $w_1+w_2+w_3=1$, are the nonnegative weights of the integrations in the objective. The objective functional can be further transformed into

$$J(\mathbf{u},p,\psi,\phi)=\int_0^T\int_\Omega [\omega_1 A(\mathbf{u},\nabla\mathbf{u},p,\psi,\nabla\psi,\phi,\nabla\phi;H(\varphi))+\omega_3\tau(\varphi)|\nabla\varphi|C(\mathbf{u},p,\psi,\phi)]\,\mathrm{d}\Omega\mathrm{d}t + \int_0^T\int_{\partial\Omega}\omega_2 B(\mathbf{u},p,\psi,\phi;H(\varphi))\,\mathrm{d}\Gamma\mathrm{d}t. \tag{3.3}$$

In the level set method, the level set function is evolved by the Hamilton-Jacobian equation [49]

$$\frac{\partial\varphi}{\partial\theta}+\mathbf{v}\cdot\nabla\varphi+v_n|\nabla\varphi|=b\kappa|\nabla\varphi| \tag{3.4}$$

where θ is the evolving time of the level set function; $\mathbf{v}$ is the evolving velocity vector; v_n is the normal evolving velocity of the level set function; b is the mean curvature evolving velocity; and κ is the mean curvature of the level set function. For the positive variational of the evolving time ($\delta\theta>0$), Eq. (3.4) is equivalent to

$$\delta\varphi=-(\mathbf{v}\cdot\nabla\varphi+v_n|\nabla\varphi|-b\kappa|\nabla\varphi|)\,\delta\theta. \tag{3.5}$$

For solving the topology optimization problem, the level set function is evolved using the Hamilton-Jacobian equation with reasonable choice of $\mathbf{v}$, v_n and b, according to the gradient information of the optimization problem.

3.2 Sensitivity analysis

The algorithm used to update the level set function in this paper belongs to the gradient based descent method. The evolving velocity is a measure of the continuum gradient of the objective to the level set function. Using the Lagrangian multiplier based adjoint

https://doi.org/10.4208/cicp.OA-2017-0003 Published online by Cambridge University Press

method, the sensitivity analysis of the topology optimization problem in Eq. (3.1) is implemented as that detailed in Appendix 5. Based on the derived sensitivity information, $\mathbf{v}$, v_n and b in the Hamilton-Jacobian equation (3.4) can respectively be chosen to be

$$\mathbf{v}=\int_0^T \nabla\left[\frac{3}{4}\sigma_0\left(1-\phi^2\right)\cos\theta_s\psi_a+\omega_3 C\right]\mathrm{d}t, \tag{3.6a}$$

$$\begin{aligned} v_n=&-\int_0^T \omega_1\frac{\partial A}{\partial H(\varphi)}-\psi\nabla\phi\cdot\mathbf{u}_a+\rho\left(\alpha_f-\alpha_s\right)\mathbf{u}\cdot\mathbf{u}_a+\left(M_f-M_s\right)\nabla\psi\cdot\nabla\phi_a\\ &-\left(\lambda_f-\lambda_s\right)\nabla\phi\cdot\nabla\psi_a-\left(\lambda_f-\lambda_s\right)\frac{1}{\epsilon^2}\phi\left(\phi^2-1\right)\mu_a\mathrm{d}t+\xi, \end{aligned} \tag{3.6b}$$

$$b=-\int_0^T\frac{3}{4}\sigma_0\left(1-\phi^2\right)\cos\theta_s\psi_a+\omega_3 C\mathrm{d}t, \tag{3.6c}$$

for maximizing the objective J; and the sign of Eq. (3.6) is reversed, for minimizing the objective J. In Eq. (3.6), $\mathbf{u}_a$, p_a, ϕ_a and ψ_a are the adjoint variables of $\mathbf{u}$, p, ϕ and ψ, respectively; and the adjoint variables are derived by solving the adjoint equations of the Navier-Stokes equations

$$\begin{aligned} &-\rho\frac{\partial\mathbf{u}_a}{\partial t}+\rho\mathbf{u}_a\cdot(\nabla\mathbf{u})-\rho(\mathbf{u}\cdot\nabla)\mathbf{u}_a+\nabla\cdot\left[-\eta\left(\nabla\mathbf{u}_a+\nabla\mathbf{u}_a^{\mathrm{T}}\right)+p_a\mathbb{I}\right]+\rho\alpha(\varphi)\mathbf{u}_a\\ &\quad+\phi_a\nabla\phi+\omega_1\frac{\partial A}{\partial\mathbf{u}}+\omega_3\tau(\varphi)|\nabla\varphi|\frac{\partial C}{\partial\mathbf{u}}-\omega_1\nabla\cdot\frac{\partial A}{\partial\nabla\mathbf{u}}=0,\quad \text{in } (0,T)\times\Omega, \end{aligned} \tag{3.7a}$$

$$-\nabla\cdot\mathbf{u}_a+\left(\omega_1\frac{\partial A}{\partial p}+\omega_3\tau(\varphi)|\nabla\varphi|\frac{\partial C}{\partial p}\right)=0,\quad \text{in } (0,T)\times\Omega, \tag{3.7b}$$

$$\mathbf{u}_a(t=T)=\mathbf{0},\quad \text{in } \Omega, \tag{3.7c}$$

$$\mathbf{u}_a=-\omega_2\frac{\partial B}{\partial p}\mathbf{n},\quad \text{on } \Gamma_{in}\cup\Gamma_{wall}, \tag{3.7d}$$

$$\left[-p_a\mathbb{I}+\eta\left(\nabla u_a+\nabla u_a^{\mathrm{T}}\right)\right]\cdot\mathbf{n}=-\rho(\mathbf{u}\cdot\mathbf{n})\mathbf{u}_a-\omega_1\frac{\partial A}{\partial\nabla\mathbf{u}}\cdot\mathbf{n},\quad \text{on } \Gamma_{out}, \tag{3.7e}$$

and the adjoint equations of the Cahn-Hilliard equations

$$\begin{aligned} &-\frac{\partial\phi_a}{\partial t}-(\mathbf{u}\cdot\nabla)\phi_a+\nabla\cdot(\lambda\nabla\psi_a)-\frac{\lambda}{\epsilon^2}\left(3\phi^2-1\right)\psi_a-\frac{3}{2}\sigma_0\phi\cos\theta_s\tau(\varphi)|\nabla\varphi|\psi_a\\ &\quad-\frac{\partial\rho}{\partial\phi}\mathbf{u}\cdot\frac{\partial\mathbf{u}_a}{\partial t}+\frac{\partial\rho}{\partial\phi}\mathbf{u}\cdot\nabla\mathbf{u}\cdot\mathbf{u}_a+\frac{\partial\eta}{\partial\phi}\left(\nabla\mathbf{u}+\nabla\mathbf{u}^{\mathrm{T}}\right):\nabla\mathbf{u}_a+\nabla\cdot[H(\varphi)\psi\mathbf{u}_a]\\ &\quad-\omega_1\nabla\cdot\frac{\partial A}{\partial\nabla\phi}+\omega_1\frac{\partial A}{\partial\phi}+\omega_3\tau(\varphi)|\nabla\varphi|\frac{\partial C}{\partial\phi}+\frac{\partial\rho}{\partial\phi}\alpha(\varphi)\mathbf{u}\cdot\mathbf{u}_a=0,\quad \text{in } (0,T)\times\Omega, \end{aligned} \tag{3.8a}$$

$$\begin{aligned} &-\nabla\cdot(M\nabla\phi_a)-\nabla\cdot\left(\omega_1\frac{\partial A}{\partial\nabla\psi}\right)\\ &\quad+\left(\psi_a+\omega_1\frac{\partial A}{\partial\psi}+\omega_3\tau(\varphi)|\nabla\varphi|\frac{\partial C}{\partial\psi}-H(\varphi)\nabla\phi\cdot\mathbf{u}_a\right)=0,\quad \text{in } (0,T)\times\Omega, \end{aligned} \tag{3.8b}$$

https://doi.org/10.4208/cicp.OA-2017-0003 Published online by Cambridge University Press

$$\phi_a = 0, \quad \text{on } \Gamma_{in}, \tag{3.8c}$$

$$-\lambda\nabla\psi_a\cdot\mathbf{n} - H(\varphi)\psi\mathbf{u}_a\cdot\mathbf{n} + \omega_1\frac{\partial A}{\partial\nabla\phi}\cdot\mathbf{n} - \frac{3}{2}\sigma\phi\cos\theta_s\psi_a - \frac{\partial\eta}{\partial\phi}\left(\nabla\mathbf{u}+\nabla\mathbf{u}^{\mathrm{T}}\right)\cdot\mathbf{u}_a\cdot\mathbf{n} + \omega_2\frac{\partial B}{\partial\phi} = 0, \quad \text{on } \Gamma_{wall}, \tag{3.8d}$$

$$-\lambda\nabla\psi_a\cdot\mathbf{n} + (\mathbf{u}\cdot\mathbf{n})\phi_a - H(\varphi)\psi\mathbf{u}_a\cdot\mathbf{n} + \omega_1\frac{\partial A}{\partial\nabla\phi}\cdot\mathbf{n} + \omega_2\frac{\partial B}{\partial\phi} = 0, \quad \text{on } \Gamma_{out}, \tag{3.8e}$$

$$M\nabla\phi_a\cdot\mathbf{n} + \omega_1\frac{\partial A}{\partial\nabla\psi}\cdot\mathbf{n} + \omega_2\frac{\partial B}{\partial\psi} = 0, \quad \text{on } \partial\Omega, \tag{3.8f}$$

$$\phi_a(t=T) = -\frac{\partial\rho}{\partial\phi}\mathbf{u}\cdot\mathbf{u}_a, \quad \text{in } \Omega. \tag{3.8g}$$

With the evolving velocity vector, normal evolving velocity and mean curvature evolving velocity in Eq. (3.6) or its reverse, the level set function can be iteratively evolved by solving the Hamilton-Jacobian equation (3.4), further the topology optimization problem in Eq. (3.1) can be solved as detailed in the following numerical test section.

4 Numerical test

4.1 Numerical implementation

The topology optimization problem of two-phase flow is solved by iteratively evolving the level set function. The procedure for the iterative evolution process includes the following steps (Table 1): 1) the coupled system of the Navier-Stokes equations and Cahn-Hilliard equations (Eq. (2.15)) are solved with the current distribution of the level set function; 2) the adjoint equations (Eqs. (3.7) and (3.8)) are solved based on the numerical solution of the coupled system; 3) the evolving velocity vector, normal evolving velocity and mean curvature evolving velocity of the level set function are computed according to Eq. (3.6) or its reverse; 4) the level set function is evolved by the Hamilton-Jacobian equation solved using upwind finite difference method. The above steps are implemented iteratively until the maximal iteration number is reached or the change of the objective values in five consecutive iterations satisfies $\frac{1}{5}\sum_{i=1}^{4}|J_{k-i}-J_{k-i-1}|/|J_k| \le 5\times10^{-2}$ in the k-th iteration, where J_k is the objective value computed in the k-th iteration. In the iterations, the Lagrangian multiplier of the volume constraint is determined using the bisection method to ensure the given volume of the fluid [64].

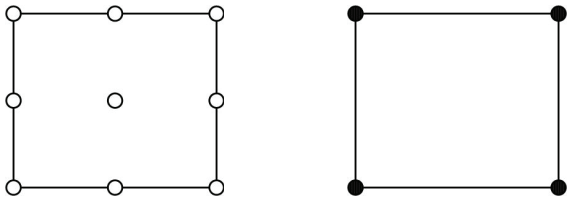
In the above procedure, the coupled equation system and the corresponding adjoint equations are solved by the finite element method implemented in the commercial finite element software COMSOL Multiphysics [59]. For the details on the numerical setting of the optimization procedure implemented in COMSOL, one can refer to [37,38]. During the optimization procedure, the Navier-Stokes equations and the adjoint equations are solved using Taylor-Hood elements, which respectively interpolate the fluidic ve-

https://doi.org/10.4208/cicp.OA-2017-0003 Published online by Cambridge University Press

Table 1: Procedure of the iterative approach for solving the topology optimization problem.

1.	Give the initial distribution of the level set function φ;
2.	Solve the coupled system of the Navier-Stokes equations and Cahn-Hilliard equations by the finite element method;
3.	Solve the adjoint equations; compute the adjoint sensitivity and the corresponding objective value;
4.	Evolve the level set function by solving the Hamilton-Jacobian equation;
5.	Check for convergence; if the stopping conditions are not satisfied, go to 2;
6.	Post processing

locity quadratically and the pressure linearly [65]; the Cahn-Hilliard equations and the corresponding adjoint equations are solved using the quadratical elements; the level set function is interpolated linearly based on the corner nodes of the elements (Fig. 3). The transient equations in the optimization are solved using the backward differentiation formula.



(a) Quadratical (b) Linear

Figure 3: Schematic for the quadratical and linear elements used in the finite element discretization. The fluid velocity $\mathbf{u}$, the phase field variable ϕ, the chemical potential ψ and their adjoints are discretized using the quadratical elements; the fluid pressure p and level set function φ are discretized using the linear elements.

To evolve the level set function, the Hamilton-Jacobin equation is solved by the upwind finite difference method on a regular mesh with ghost elements (Fig. 4). The support size h of the smoothed Heaviside function and Dirac function is set to be the size of the regular mesh. The time step for the finite difference scheme is chosen based on the CFL stability condition [66]

$$\Delta\theta \leq \frac{\beta h_E}{\max\left\{\left|\mathbf{v}\cdot\mathbf{n}_\varphi + v_n - b\kappa\right|\right\}}, \quad \text{where } \beta \in (0,1), \tag{4.1}$$

where $\mathbf{n}_\varphi = \frac{\nabla\varphi}{|\nabla\varphi|}$ is the unit normal vector of the level set function; h_E is the size of the elements and β is chosen to be 0.1 in this paper. The evolved level set function is reinitialized after several time steps. The reinitialization of the level set function is performed by solving the Hamilton-Jacobin equation without explicitly determining the zero

https://doi.org/10.4208/cicp.OA-2017-0003 Published online by Cambridge University Press

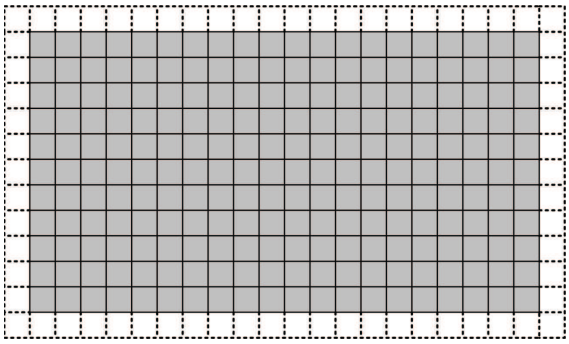


Figure 4: Schematic for the grid mesh with ghost elements. The solid mesh is used to solve the Navier-Stokes equations and the Cahn-Hilliard equations; the combination of the solid and dash meshes is used to solve the Hamilton-Jacobian equation for evolving the level set function.

level set [66]

$$\frac{\partial \varphi}{\partial \theta} = \text{sign}(\varphi_0)(1-|\nabla \varphi|), \tag{4.2}$$

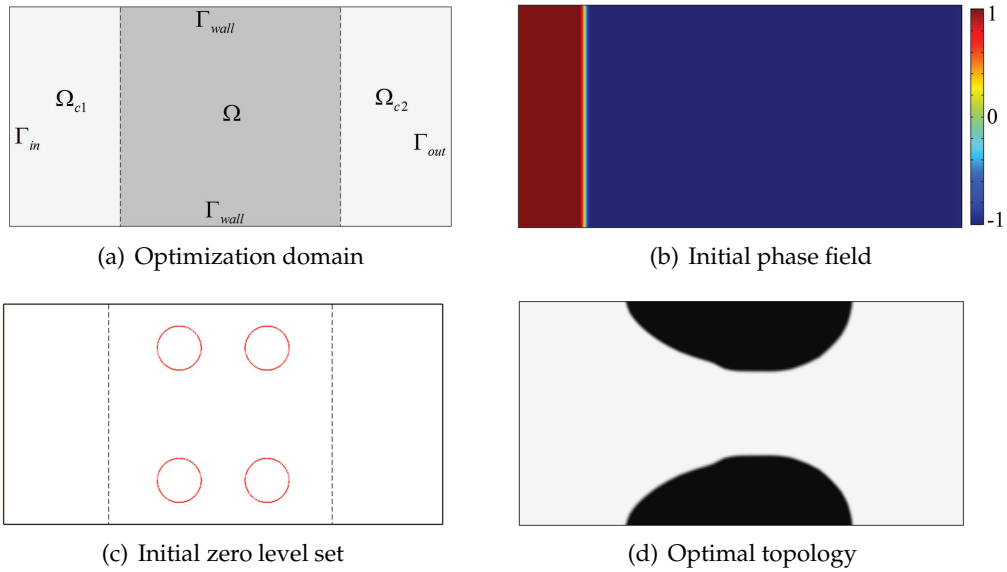
where $\text{sign}(\varphi_0)$ denotes the sign value of the un-initialized level set function φ_0, which is either 1, -1 or 0. Eq. (4.2) is also solved using the upwind finite difference method on the regular mesh with ghost elements as shown in Fig. 4.

4.2 Numerical examples

To demonstrate the performance of the proposed topology optimization method for two-phase flow, topology optimization of the connection of two capillaries is provided as follows. In the optimization of the connection, the cost functional is chosen to maximize the kinetic energy of the fluids in the capillary, i.e. A is set to be $\frac{1}{2}\rho \mathbf{u}^2 H(\varphi)$ with the coefficient ω_1 equal to 1. The computational domain, the initial distribution of the phase field variable and the initial distribution of the zero level set are respectively set as shown in Fig. 5(a)-(c). The size of the rectangular computational domain is set to be $200\times 100\mu\text{m}^2$, with square optimization domain sized $100\times 100\mu\text{m}^2$. The level set function is evolved 10 time steps in every iteration, and it is re-initialized after every 10 iterations. The maximal iteration number is set to be 600. When the two fluids in the optimization domain are respectively set to be water and air with density ratio 1×10^3 and dynamic viscosity ratio 1×10^2. The physical and optimization parameters are listed in Table 2. The terminal time of the capillary is set to be $T = 1.2\times 10^{-4}$. Then the optimal design of the capillary connection is obtained as shown in Fig. 5(d). Snapshots for the evolution of the zero level set and level set function are shown in Fig. 6. And the convergent histories of the objective value and volume fraction are shown in Fig. 7.

To further demonstrate the robustness of the outlined topology optimization method for two-phase flow, the initial zero level set for the topology optimization of capillary connection is changed to be the one shown in Fig. 8(a). Correspondingly, snapshots for

https://doi.org/10.4208/cicp.OA-2017-0003 Published online by Cambridge University Press



(a) Optimization domain (b) Initial phase field

(c) Initial zero level set (d) Optimal topology

Figure 5: (a) Optimization domain of the capillary connection, where Ω is the optimization domain, Ω_{c1} and Ω_{c2} are capillaries connected to the optimization domain; (b) initial distribution of the phase field variable; (c) initial distribution of the zero level set in the design domain Ω; (d) optimal topology of the capillary connection obtained by the outline topology optimization method for two-phase flow.

Table 2: Parameter setting for the topology optimization of the capillary connection.

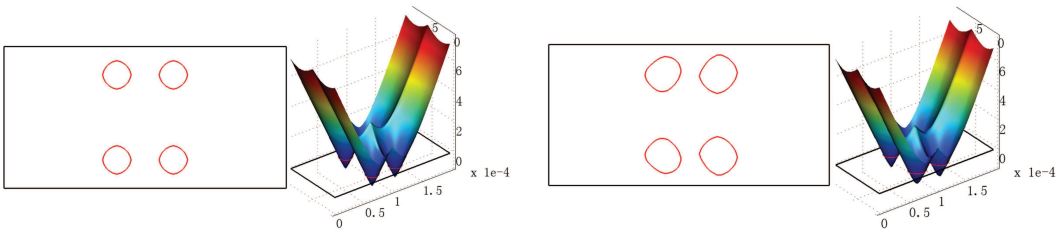
$\rho_1\ (kg/m^3)$	$\rho_2\ (kg/m^3)$	$\eta_1\ (Pa\cdot s)$	$\eta_2\ (Pa\cdot s)$	M_f	M_s
1×10^{3}	1×10^{0}	1×10^{-3}	1×10^{-5}	1×10^{0}	1×10^{3}

$\lambda_f\ (N/m^2)$	$\lambda_s\ (N/m^2)$	$\epsilon\ (m)$	$\sigma_0\ (N/m)$	$\theta_s\ (rad)$	$\alpha_s\ (kg/s)$
1×10^{0}	1×10^{-3}	2.5×10^{-6}	7.2×10^{-2}	$\pi/4$	1×10^{7}

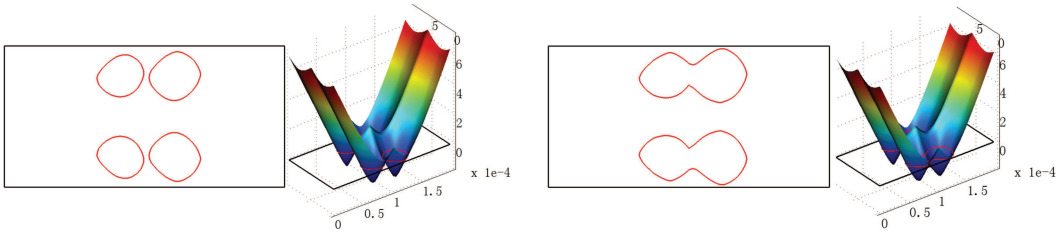
the evolution of the zero level set and level set function are shown in Fig. 8, where the same optimal topology is obtained for the capillary connection.

In the derived topology (Fig. 5(d)), the inlet part of the connection has the shape with smooth size-shrinking, which can increase the curvature of the capillary interface. As demonstrated in Young-Laplace equation used to describe the capillary pressure difference sustained across the interface between two immiscible fluids [70, 71], the capillary pressure difference is proportional to the curvature of the capillary interface. Then the shape of the inlet part is to increase the capillary pressure difference and enhance the driving effect of the surface tension. Meanwhile, the outlet part of the derived connection smoothes over the sudden size change between the connection and right capillary. This removes the contact angle anchoring, which occurs as the capillary interface passing the position with sudden size-expanding. Therefore, the kinetic energy of the fluids is maximized in the derived connection with the sequential performance on increasing the

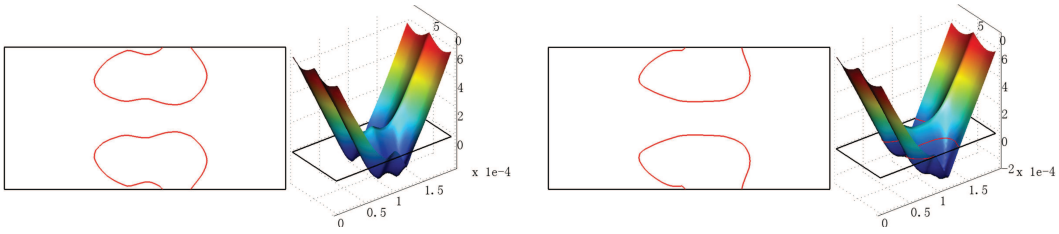
https://doi.org/10.4208/cicp.OA-2017-0003 Published online by Cambridge University Press



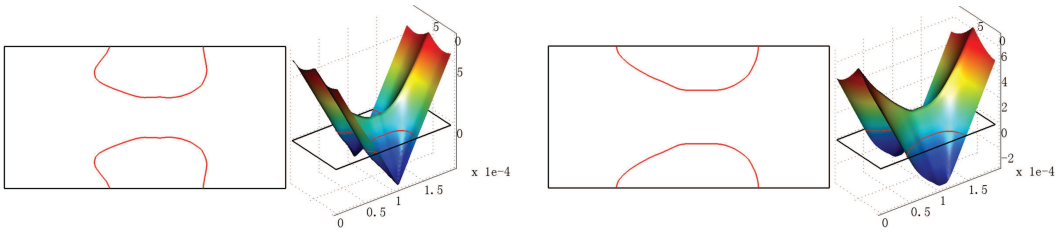
(a) Initial (b) Iteration 10



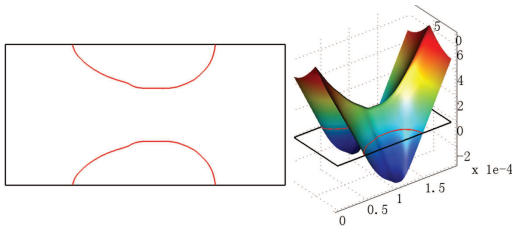
(c) Iteration 17 (d) Iteration 20



(e) Iteration 30 (f) Iteration 60



(g) Iteration 100 (h) Iteration 200



(i) Iteration 580

Figure 6: Snapshots for the evolution of the zero level set and the corresponding level set function.

https://doi.org/10.4208/cicp.OA-2017-0003 Published online by Cambridge University Press

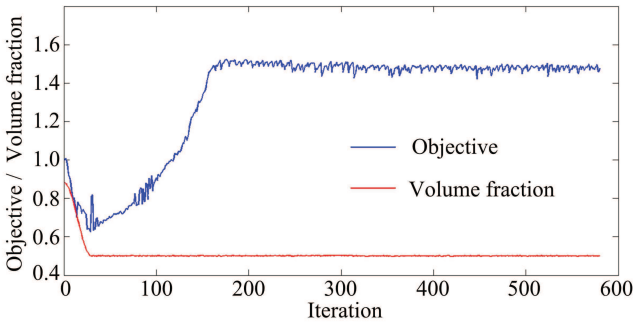


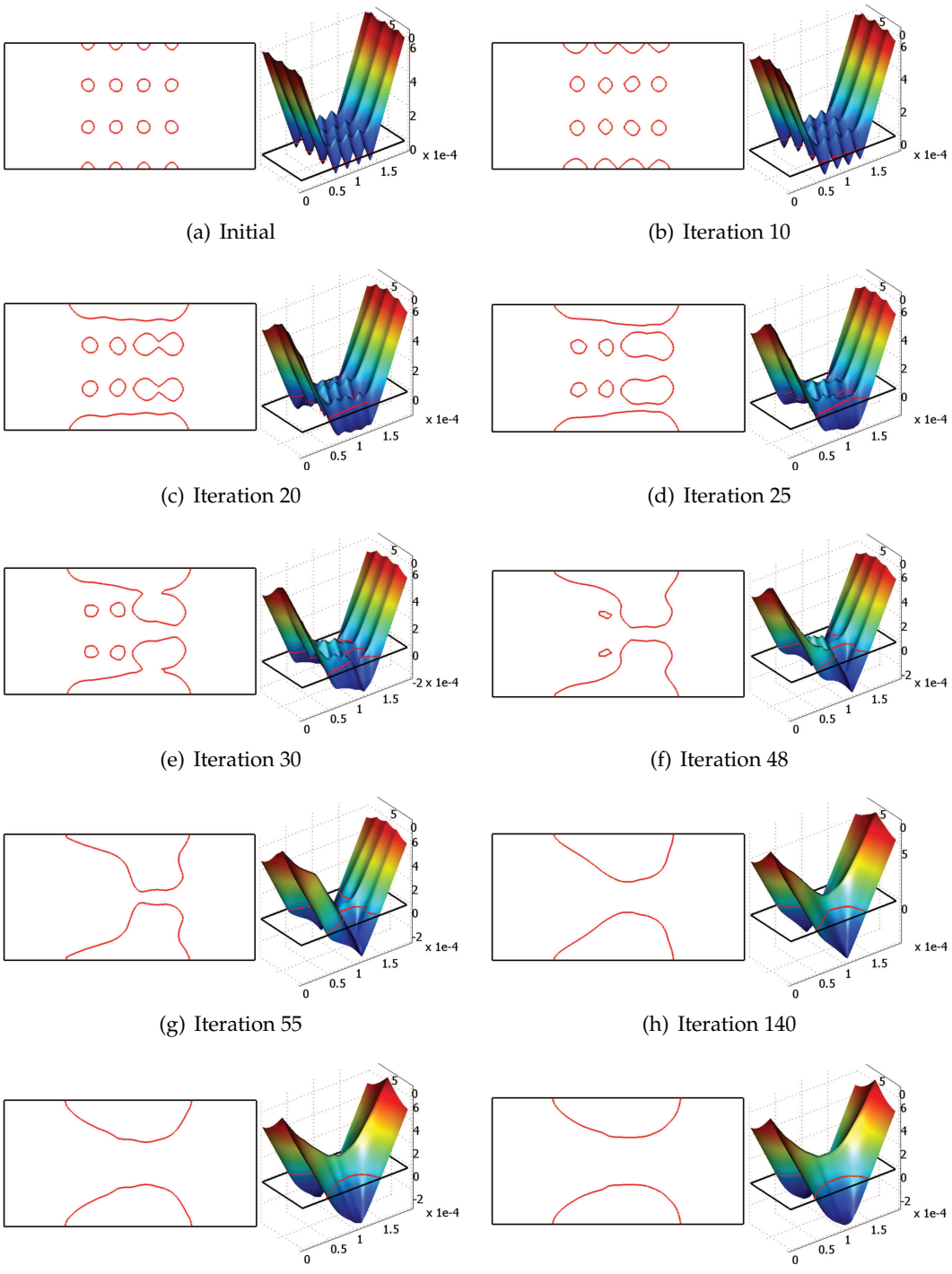
Figure 7: Convergence histories of the objective value and volume fraction.

curvature of the capillary interface and removing the contact angle anchoring. This analysis can be confirmed by the snapshots for the evolution of the capillary interface in the optimized connection shown in Fig. 9, which demonstrates that the optimized connection keeps the driving effect of the surface tension, makes the surface tension do positive work and maximizes the kinetic energy of the fluids.

5 Conclusions

This paper has presented the topology optimization method for the two-phase flow with two immiscible fluids. In the developed method, the diffuse-interface model with essential no slip boundary condition is chosen to describe the two-phase flow, and further to ensure the applicability of the fluid velocity penalization method, because the singularity at the contact line of the two-phase flow is regularized by the Cahn-Hilliard diffusion instead of slip boundary condition with velocity slip. To avoid the artificial fluid flow driven by the interfacial tension in the implicit solid phase and keep the interfacial tension in the fluid phase, the surface tension term in the Navier-Stokes equations is penalized by the Heaviside of the level set function. To express the wall energy at the implicit solid-fluid interface, the level set method, which can exactly express the normal vector and curvature of the implicit fluid-solid interface, is chosen to implement the topology optimization of two-phase flow. Based on the total free energy of the two-phase flow, the Cahn-Hilliard equations are modified to govern the phase field of the diffuse-interface model defined on the fluid and solid phases implicitly expressed by the level set function. Then the level set method based variational problem, constrained by the coupled system of the Navier-Stokes equations and the Cahn-Hilliard equations, is constructed and analyzed for the topology optimization of two-phase flow. Numerical examples, with topology optimization of the connection between two capillaries, demonstrate the robustness of the proposed topology optimization method for two-phase flow. And the proposed method has extended topology optimization into the area of two-phase flow, and it can provide the designers a more reasonable design tool in engineering requirement on the control of two-phase flows.

https://doi.org/10.4208/cicp.OA-2017-0003 Published online by Cambridge University Press



(a) Initial (b) Iteration 10

(c) Iteration 20 (d) Iteration 25

(e) Iteration 30 (f) Iteration 48

(g) Iteration 55 (h) Iteration 140

(i) Iteration 180 (j) Iteration 255

Figure 8: Snapshots for the evolution of the zero level set and the corresponding level set function when the initial level set function is set to be the one shown in Fig. 8(a).

https://doi.org/10.4208/cicp.OA-2017-0003 Published online by Cambridge University Press

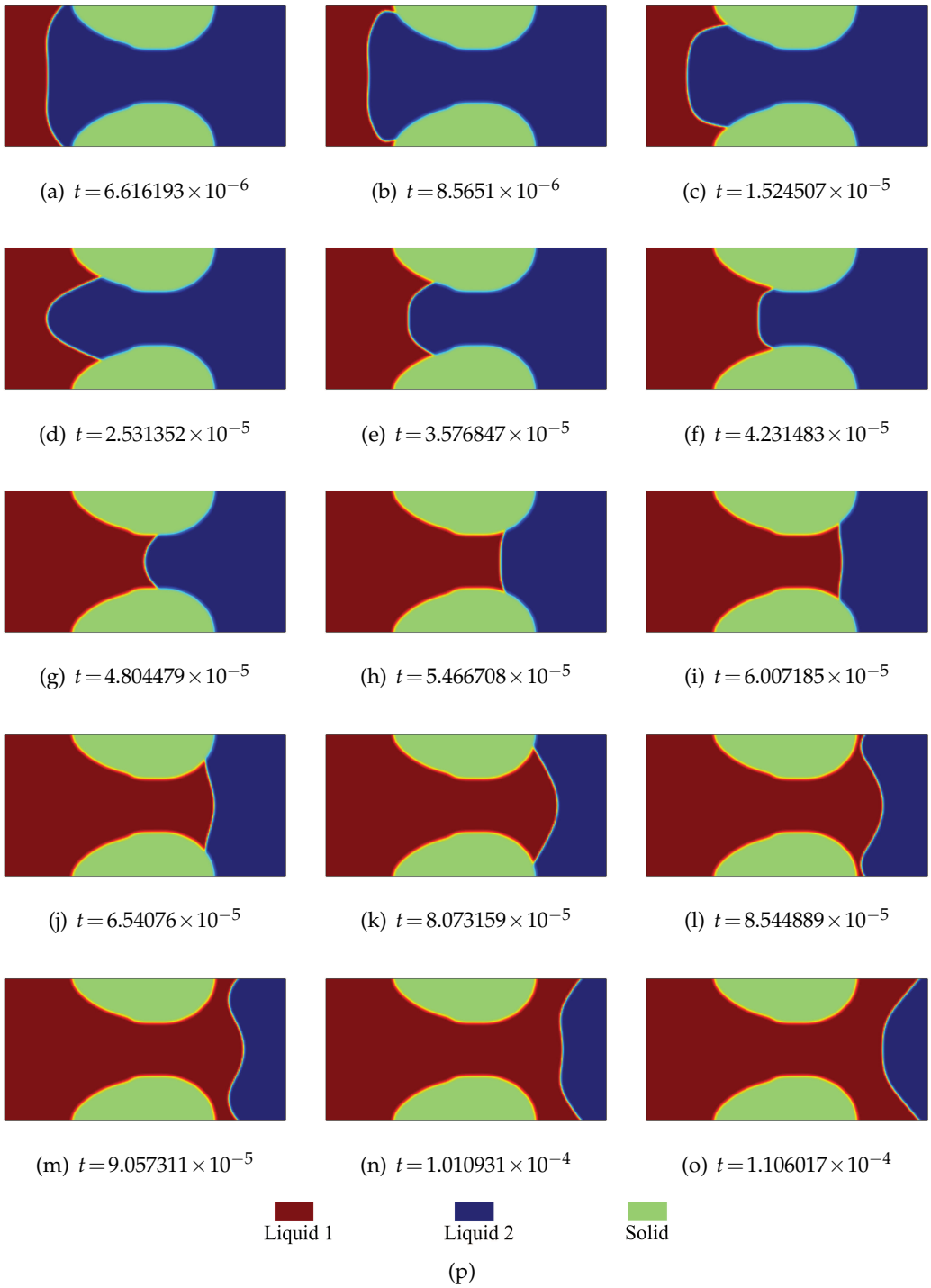


Figure 9: Snapshots for the evolution of the capillary interface in the optimized capillary connection.

https://doi.org/10.4208/cicp.OA-2017-0003 Published online by Cambridge University Press

Appendix

The Lagrangian multiplier based adjoint method are used to perform the sensitivity analysis of the topology optimization problem in Eq. (3.1) [67–69]. According to the Lagrangian multiplier based adjoint method, the augmented Lagrangian corresponding to the optimization problem in Eq. (3.1) can be introduced as

$$\hat{J}=J(\mathbf{u},p,\psi,\phi;\varphi)+e(\mathbf{u},p,\psi,\phi;\varphi)-\xi\left(\int_\Omega H(\varphi)\,\mathrm{d}\Omega-V^*V_0\right), \tag{A.1}$$

where

$$\begin{aligned}
&e(\mathbf{u},p,\psi,\phi;\varphi)\\
=&\int_\Omega[\rho\mathbf{u}\cdot\mathbf{u}_a]_{t=0}^{t=T}\,\mathrm{d}\Omega+\int_0^T\int_\Omega-\rho\mathbf{u}\cdot\frac{\partial\mathbf{u}_a}{\partial t}+(\rho\mathbf{u}\cdot\nabla\mathbf{u})\cdot\mathbf{u}_a\\
&+\left[-p\mathbb{I}+\eta\left(\nabla\mathbf{u}+\nabla\mathbf{u}^{\mathrm{T}}\right)\right]:\nabla\mathbf{u}_a-H(\varphi)\psi\nabla\phi\cdot\mathbf{u}_a+\rho\alpha(\varphi)\mathbf{u}\cdot\mathbf{u}_a-p_a\nabla\cdot\mathbf{u}\,\mathrm{d}\Omega\mathrm{d}t\\
&+\int_0^T\int_{\partial\Omega}-\left[-p\mathbb{I}+\eta\left(\nabla\mathbf{u}+\nabla\mathbf{u}^{\mathrm{T}}\right)\right]\cdot\mathbf{u}_a\cdot\mathbf{n}\,\mathrm{d}\Gamma\mathrm{d}t+\int_\Omega[\phi\phi_a]_{t=0}^{t=T}\,\mathrm{d}\Omega\\
&+\int_0^T\int_\Omega-\phi\frac{\partial\phi_a}{\partial t}+(\mathbf{u}\cdot\nabla\phi)\phi_a+M(\varphi)\nabla\psi\cdot\nabla\phi_a\,\mathrm{d}\Omega\mathrm{d}t\\
&+\int_0^T\int_\Omega\psi\psi_a-\lambda(\varphi)\nabla\phi\cdot\nabla\psi_a-\frac{\lambda(\varphi)}{\epsilon^2}\phi\left(\phi^2-1\right)\psi_a\\
&+\frac{3}{4}\sigma_0\left(1-\phi^2\right)\cos\theta_s\tau(\varphi)|\nabla\varphi|\psi_a\,\mathrm{d}\Omega\mathrm{d}t+\int_0^T\int_{\Gamma_{in}\cup\Gamma_{wall}}\lambda(\varphi)\nabla\phi\cdot\mathbf{n}\psi_a\,\mathrm{d}\Gamma\mathrm{d}t,
\end{aligned} \tag{A.2}$$

$\mathbf{u}_a$, p_a, ϕ_a and ψ_a are the adjoint variables of $\mathbf{u}$, p, ϕ and ψ, respectively; ϕ, ψ, ϕ_a, ψ_a, and the components of $\mathbf{u}$ and $\mathbf{u}_a$ are valued in the functional space $L^2\left((0,T);H^1(\Omega)\right)$; p and p_a are valued in $L^2\left((0,T);L^2(\Omega)\right)$; L^2 is the second-order integrable Lebesgue space; H^1 is the first-order Sobolev space; the fluid volume constraint is dealt with the Lagrangian multiplier method, and ξ is the corresponding Lagrangian multiplier. According to Karush-Kuhn-Tucker conditions of partial differential equation constrained optimization problem [68], the variational of $\hat{J}$

$$\delta\hat{J}=\left\langle\frac{\partial J}{\partial\mathbf{u}},\delta\mathbf{u}\right\rangle+\left\langle\frac{\partial J}{\partial p},\delta p\right\rangle+\left\langle\frac{\partial J}{\partial\phi},\delta\phi\right\rangle+\left\langle\frac{\partial J}{\partial\psi},\delta\psi\right\rangle+\left\langle\frac{\partial J}{\partial\varphi},\delta\varphi\right\rangle \tag{A.3}$$

should be zero at the optimal distribution of the level set function. Therefore, the adjoint equations can be derived based on the following equations

$$\left\langle\frac{\partial J}{\partial\mathbf{u}},\delta\mathbf{u}\right\rangle=0;\quad\left\langle\frac{\partial J}{\partial p},\delta p\right\rangle=0;\quad\left\langle\frac{\partial J}{\partial\phi},\delta\phi\right\rangle=0;\quad\left\langle\frac{\partial J}{\partial\psi},\delta\psi\right\rangle=0. \tag{A.4}$$

https://doi.org/10.4208/cicp.OA-2017-0003 Published online by Cambridge University Press

The variational of the augmented Lagrangian is

$$
\begin{aligned}
\delta\hat{J}=&\int_0^T\int_\Omega\left[\omega_1\left(\frac{\partial A}{\partial\mathbf{u}}-\nabla\cdot\frac{\partial A}{\partial\nabla\mathbf{u}}\right)+\omega_3\tau(\varphi)|\nabla\varphi|\frac{\partial C}{\partial\mathbf{u}}\right]\cdot\delta\mathbf{u}\,\mathrm{d}\Omega\mathrm{d}t\\
&+\int_0^T\int_{\partial\Omega}\omega_1\frac{\partial A}{\partial\nabla\mathbf{u}}\cdot\mathbf{n}\cdot\delta\mathbf{u}\,\mathrm{d}\Gamma\mathrm{d}t+\int_0^T\int_\Omega\left[\omega_1\frac{\partial A}{\partial p}+\omega_3\tau(\varphi)|\nabla\varphi|\frac{\partial C}{\partial p}\right]\delta p\,\mathrm{d}\Omega\mathrm{d}t\\
&+\int_0^T\int_\Omega\left[\omega_1\left(\frac{\partial A}{\partial\psi}-\nabla\cdot\frac{\partial A}{\partial\nabla\psi}\right)+\omega_3\tau(\varphi)|\nabla\varphi|\frac{\partial C}{\partial\psi}\right]\delta\psi\,\mathrm{d}\Omega\mathrm{d}t\\
&+\int_0^T\int_{\partial\Omega}\omega_1\frac{\partial A}{\partial\nabla\psi}\cdot\mathbf{n}\delta\psi\,\mathrm{d}\Gamma\mathrm{d}t+\int_0^T\int_\Omega\left[\omega_1\left(\frac{\partial A}{\partial\phi}-\nabla\cdot\frac{\partial A}{\partial\nabla\phi}\right)+\omega_3\tau(\varphi)|\nabla\varphi|\frac{\partial C}{\partial\phi}\right]\delta\phi\,\mathrm{d}\Omega\mathrm{d}t\\
&+\int_0^T\int_{\partial\Omega}\omega_1\frac{\partial A}{\partial\nabla\phi}\cdot\mathbf{n}\delta\phi\,\mathrm{d}\Gamma\mathrm{d}t+\int_0^T\int_\Omega\left[\omega_1\frac{\partial A}{\partial H(\varphi)}\tau(\varphi)+\omega_3\frac{\partial(\tau(\varphi)|\nabla\varphi|)}{\partial\varphi}C\right]\delta\varphi\,\mathrm{d}\Omega\mathrm{d}t\\
&+\int_0^T\int_{\partial\Omega}\omega_2\left[\frac{\partial B}{\partial\mathbf{u}}\delta\mathbf{u}+\frac{\partial B}{\partial p}\delta p+\frac{\partial B}{\partial\psi}\delta\psi+\frac{\partial B}{\partial\phi}\delta\phi+\frac{\partial B}{\partial H(\varphi)}\tau(\varphi)\delta\varphi\right]\mathrm{d}\Gamma\mathrm{d}t\\
&+\int_\Omega\left[\rho\delta\mathbf{u}\cdot\mathbf{u}_a+\frac{\partial\rho}{\partial\phi}\mathbf{u}\cdot\mathbf{u}_a\delta\phi\right]_{t=T}\mathrm{d}\Omega+\int_0^T\int_\Omega-\rho\delta\mathbf{u}\cdot\frac{\partial\mathbf{u}_a}{\partial t}-\frac{\partial\rho}{\partial\phi}\mathbf{u}\cdot\frac{\partial\mathbf{u}_a}{\partial t}\delta\phi\\
&+(\rho\delta\mathbf{u}\cdot\nabla\mathbf{u})\cdot\mathbf{u}_a+(\rho\mathbf{u}\cdot\nabla\delta\mathbf{u})\cdot\mathbf{u}_a+\left(\frac{\partial\rho}{\partial\phi}\mathbf{u}\cdot\nabla\mathbf{u}\right)\cdot\mathbf{u}_a\delta\phi+\left[-\delta p\mathbb{I}+\eta\left(\nabla\delta\mathbf{u}+\nabla\delta\mathbf{u}^{\mathrm{T}}\right)\right]:\nabla\mathbf{u}_a\\
&+\left[\frac{\partial\eta}{\partial\phi}\left(\nabla\mathbf{u}+\nabla\mathbf{u}^{\mathrm{T}}\right)\right]:\nabla\mathbf{u}_a\delta\phi-H(\varphi)\psi\nabla\delta\phi\cdot\mathbf{u}_a-H(\varphi)\delta\psi\nabla\phi\cdot\mathbf{u}_a-\tau(\varphi)\psi\nabla\phi\cdot\mathbf{u}_a\delta\varphi\\
&+\rho\alpha(\varphi)\delta\mathbf{u}\cdot\mathbf{u}_a+\frac{\partial\rho}{\partial\phi}\alpha(\varphi)\mathbf{u}\cdot\mathbf{u}_a\delta\phi+\rho\frac{\partial\alpha(\varphi)}{\partial\varphi}\mathbf{u}\cdot\mathbf{u}_a\delta\varphi-p_a\nabla\cdot\delta\mathbf{u}\,\mathrm{d}\Omega\mathrm{d}t\\
&+\int_0^T\int_{\Gamma_{in}\cup\Gamma_{wall}}\mathbf{u}_a\cdot\mathbf{n}\delta p-\frac{\partial\eta}{\partial\phi}\left(\nabla\mathbf{u}+\nabla\mathbf{u}^{\mathrm{T}}\right)\cdot\mathbf{u}_a\cdot\mathbf{n}\delta\phi\,\mathrm{d}\Gamma\mathrm{d}t+\int_\Omega\left[\phi_a\delta\phi\right]_{t=T}\mathrm{d}\Omega\\
&+\int_0^T\int_\Omega-\delta\phi\frac{\partial\phi_a}{\partial t}+(\delta\mathbf{u}\cdot\nabla\phi)\phi_a+(\mathbf{u}\cdot\nabla\delta\phi)\phi_a+\frac{\partial M}{\partial\varphi}\nabla\psi\cdot\nabla\phi_a\delta\varphi+M\nabla\delta\psi\cdot\nabla\phi_a\,\mathrm{d}\Omega\mathrm{d}t\\
&+\int_0^T\int_\Omega\delta\psi\psi_a-\lambda\nabla\delta\phi\cdot\nabla\psi_a-\frac{\partial\lambda}{\partial\varphi}\nabla\phi\cdot\nabla\psi_a\delta\varphi-\frac{\lambda}{\epsilon^2}\left(3\phi^2-1\right)\psi_a\delta\phi\\
&-\frac{\partial\lambda}{\partial\varphi}\frac{1}{\epsilon^2}\phi\left(\phi^2-1\right)\psi_a\delta\varphi-\frac{3}{2}\sigma_0\phi\cos\theta_s\tau(\varphi)|\nabla\varphi|\psi_a\delta\phi+\frac{3}{4}\sigma_0\left(1-\phi^2\right)\cos\theta_s\frac{\partial(\tau(\varphi)|\nabla\varphi|)}{\partial\varphi}\\
&\psi_a\delta\varphi\,\mathrm{d}\Omega\mathrm{d}t+\int_0^T\int_{\Gamma_{in}}\lambda\nabla\delta\phi\cdot\mathbf{n}\psi_a+\frac{\partial\lambda}{\partial\varphi}\nabla\phi\cdot\mathbf{n}\psi_a\delta\varphi\,\mathrm{d}\Gamma\mathrm{d}t+\int_0^T\int_{\Gamma_{wall}}-\frac{3}{2}\sigma\phi\cos\theta_s\psi_a\delta\phi\\
&+\frac{\sqrt{2}}{2}\frac{\lambda_h-\lambda_l}{\epsilon}\left(1-\phi^2\right)\cos\theta_s\tau(\varphi)\psi_a\delta\varphi\,\mathrm{d}\Gamma\mathrm{d}t+\int_\Omega-\xi\tau(\varphi)\delta\varphi\,\mathrm{d}\Omega. \qquad \text{(A.5)}
\end{aligned}
$$

Then based on the first two formulas in Eq. (A.4), the weak form of the adjoint equations for the Navier-Stokes equations is derived as

https://doi.org/10.4208/cicp.OA-2017-0003 Published online by Cambridge University Press

$$\int_0^T\int_\Omega -\rho\delta\mathbf{u}\cdot\frac{\partial\mathbf{u}_a}{\partial t}+(\rho\delta\mathbf{u}\cdot\nabla\mathbf{u})\cdot\mathbf{u}_a+(\rho\mathbf{u}\cdot\nabla\delta\mathbf{u})\cdot\mathbf{u}_a+\left[-\delta p\mathbb{I}+\eta\left(\nabla\delta\mathbf{u}+\nabla\delta\mathbf{u}^{\mathrm{T}}\right)\right]:\nabla\mathbf{u}_a$$
$$+\rho\alpha(\varphi)\delta\mathbf{u}\cdot\mathbf{u}_a-p_a\nabla\cdot\delta\mathbf{u}+(\delta\mathbf{u}\cdot\nabla\phi)\phi_a+\left(\omega_1\frac{\partial A}{\partial p}+\omega_3\tau(\varphi)|\nabla\varphi|\frac{\partial C}{\partial p}\right)\cdot\delta p$$
$$+\left(\omega_1\frac{\partial A}{\partial\mathbf{u}}+\omega_3\tau(\varphi)|\nabla\varphi|\frac{\partial C}{\partial\mathbf{u}}\right)\cdot\delta\mathbf{u}+\omega_1\frac{\partial A}{\partial\nabla\mathbf{u}}:\nabla\delta\mathbf{u}\,\mathrm{d}\Omega\mathrm{d}t$$
$$+\int_0^T\int_{\Gamma_{in}\cup\Gamma_{wall}}\left(\mathbf{u}_a\cdot\mathbf{n}+\omega_2\frac{\partial B}{\partial p}\right)\delta p\,\mathrm{d}\Gamma\mathrm{d}t+\int_0^T\int_{\Gamma_{out}}\omega_2\frac{\partial B}{\partial\mathbf{u}}\cdot\delta\mathbf{u}\,\mathrm{d}\Gamma\mathrm{d}t=0; \tag{A.6a}$$

$$\mathbf{u}_a(t=T)=\mathbf{0},\quad \text{in }\Omega, \tag{A.6b}$$

And the corresponding strong form of the adjoint equations for the Navier-Stokes equations is

$$-\rho\frac{\partial\mathbf{u}_a}{\partial t}+\rho\mathbf{u}_a\cdot(\nabla\mathbf{u})-\rho(\mathbf{u}\cdot\nabla)\mathbf{u}_a+\nabla\cdot\left[-\eta\left(\nabla\mathbf{u}_a+\nabla\mathbf{u}_a^{\mathrm{T}}\right)+p_a\mathbb{I}\right]+\rho\alpha(\varphi)\mathbf{u}_a+\phi_a\nabla\phi$$
$$+\omega_1\frac{\partial A}{\partial\mathbf{u}}+\omega_3\tau(\varphi)|\nabla\varphi|\frac{\partial C}{\partial\mathbf{u}}-\omega_1\nabla\cdot\frac{\partial A}{\partial\nabla\mathbf{u}}=0,\quad \text{in }(0,T)\times\Omega, \tag{A.7a}$$

$$-\nabla\cdot\mathbf{u}_a+\left(\omega_1\frac{\partial A}{\partial p}+\omega_3\tau(\varphi)|\nabla\varphi|\frac{\partial C}{\partial p}\right)=0,\quad \text{in }(0,T)\times\Omega, \tag{A.7b}$$

$$\mathbf{u}_a(t=T)=\mathbf{0},\quad \text{in }\Omega, \tag{A.7c}$$

$$\mathbf{u}_a=-\omega_2\frac{\partial B}{\partial p}\mathbf{n},\quad \text{on }\Gamma_{in}\cup\Gamma_{wall}, \tag{A.7d}$$

$$\left[-p_a\mathbb{I}+\eta\left(\nabla u_a+\nabla u_a^{\mathrm{T}}\right)\right]\cdot\mathbf{n}=-\rho(\mathbf{u}\cdot\mathbf{n})\mathbf{u}_a-\omega_1\frac{\partial A}{\partial\nabla\mathbf{u}}\cdot\mathbf{n},\quad \text{on }\Gamma_{out}. \tag{A.7e}$$

Based on the third and fourth formulas in Eq. (A.4), the weak form of the adjoint equation for the Cahn-Hilliard equations is derived as

$$\int_0^T\int_\Omega -\delta\phi\frac{\partial\phi_a}{\partial t}+(\mathbf{u}\cdot\nabla\delta\phi)\phi_a-\lambda\nabla\delta\phi\cdot\nabla\psi_a-\frac{\lambda}{\epsilon^2}\left(3\phi^2-1\right)\psi_a\delta\phi$$
$$-\frac{3}{2}\sigma_0\phi\cos\theta_s\tau(\varphi)|\nabla\varphi|\psi_a\delta\phi-\frac{\partial\rho}{\partial\phi}\mathbf{u}\cdot\frac{\partial\mathbf{u}_a}{\partial t}\delta\phi+\frac{\partial\rho}{\partial\phi}\mathbf{u}\cdot\nabla\mathbf{u}\cdot\mathbf{u}_a\delta\phi$$
$$+\frac{\partial\eta}{\partial\phi}\left(\nabla\mathbf{u}+\nabla\mathbf{u}^{\mathrm{T}}\right):\nabla\mathbf{u}_a\delta\phi-H(\varphi)\psi\nabla\delta\phi\cdot\mathbf{u}_a+\omega_1\frac{\partial A}{\partial\nabla\phi}\cdot\nabla\delta\phi$$
$$+\left(\omega_1\frac{\partial A}{\partial\phi}+\omega_3\tau(\varphi)|\nabla\varphi|\frac{\partial C}{\partial\phi}\right)\delta\phi+\frac{\partial\rho}{\partial\phi}\alpha(\varphi)\mathbf{u}\cdot\mathbf{u}_a\delta\phi\,\mathrm{d}\Omega\mathrm{d}t$$
$$+\int_0^T\int_{\Gamma_{in}}\lambda\nabla\delta\phi\cdot\mathbf{n}\psi_a-\frac{\partial\eta}{\partial\phi}\left(\nabla\mathbf{u}+\nabla\mathbf{u}^{\mathrm{T}}\right)\cdot\mathbf{u}_a\cdot\mathbf{n}\delta\phi\,\mathrm{d}\Gamma\mathrm{d}t+\int_0^T\int_{\Gamma_{wall}}-\frac{3}{2}\sigma\phi\cos\theta_s\psi_a\delta\phi$$

https://doi.org/10.4208/cicp.OA-2017-0003 Published online by Cambridge University Press

$$-\frac{\partial\eta}{\partial\phi}\left(\nabla\mathbf{u}+\nabla\mathbf{u}^{\mathrm{T}}\right)\cdot\mathbf{u}_a\cdot\mathbf{n}\delta\phi+\omega_2\frac{\partial B}{\partial\phi}\delta\phi\mathrm{d}\Gamma\mathrm{d}t+\int_0^T\int_{\Gamma_{out}}\omega_2\frac{\partial B}{\partial\phi}\delta\phi\mathrm{d}\Gamma\mathrm{d}t+\int_0^T\int_\Omega M\nabla\delta\psi\cdot\nabla\phi_a$$
$$+\omega_1\frac{\partial A}{\partial\nabla\psi}\cdot\nabla\delta\psi+\left(\psi_a+\omega_1\frac{\partial A}{\partial\psi}+\omega_3\tau(\varphi)|\nabla\varphi|\frac{\partial C}{\partial\psi}-H(\varphi)\nabla\phi\cdot\mathbf{u}_a\right)\delta\psi\mathrm{d}\Omega\mathrm{d}t$$
$$+\int_0^T\int_{\partial\Omega}\omega_2\frac{\partial B}{\partial\psi}\delta\psi\mathrm{d}\Gamma\mathrm{d}t=0; \tag{A.8a}$$

$$\phi_a(t=T)=-\frac{\partial\rho}{\partial\phi}\mathbf{u}\cdot\mathbf{u}_a,\quad\text{in }\Omega. \tag{A.8b}$$

And the corresponding strong form is

$$-\frac{\partial\phi_a}{\partial t}-(\mathbf{u}\cdot\nabla)\phi_a+\nabla\cdot(\lambda\nabla\psi_a)-\frac{\lambda}{\epsilon^2}\left(3\phi^2-1\right)\psi_a-\frac{3}{2}\sigma_0\phi\cos\theta_s\tau(\varphi)|\nabla\varphi|\psi_a$$
$$-\frac{\partial\rho}{\partial\phi}\mathbf{u}\cdot\frac{\partial\mathbf{u}_a}{\partial t}+\frac{\partial\rho}{\partial\phi}\mathbf{u}\cdot\nabla\mathbf{u}\cdot\mathbf{u}_a+\frac{\partial\eta}{\partial\phi}\left(\nabla\mathbf{u}+\nabla\mathbf{u}^{\mathrm{T}}\right):\nabla\mathbf{u}_a+\nabla\cdot[H(\varphi)\psi\mathbf{u}_a]-\omega_1\nabla\cdot\frac{\partial A}{\partial\nabla\phi}$$
$$+\omega_1\frac{\partial A}{\partial\phi}+\omega_3\tau(\varphi)|\nabla\varphi|\frac{\partial C}{\partial\phi}+\frac{\partial\rho}{\partial\phi}\alpha(\varphi)\mathbf{u}\cdot\mathbf{u}_a=0,\quad\text{in }(0,T)\times\Omega, \tag{A.9a}$$

$$-\nabla\cdot(M\nabla\phi_a)-\nabla\cdot\left(\omega_1\frac{\partial A}{\partial\nabla\psi}\right)$$
$$+\left(\psi_a+\omega_1\frac{\partial A}{\partial\psi}+\omega_3\tau(\varphi)|\nabla\varphi|\frac{\partial C}{\partial\psi}-H(\varphi)\nabla\phi\cdot\mathbf{u}_a\right)=0,\quad\text{in }(0,T)\times\Omega, \tag{A.9b}$$

$$\phi_a=0,\quad\text{on }\Gamma_{in}, \tag{A.9c}$$

$$-\lambda\nabla\psi_a\cdot\mathbf{n}-H(\varphi)\psi\mathbf{u}_a\cdot\mathbf{n}+\omega_1\frac{\partial A}{\partial\nabla\phi}\cdot\mathbf{n}-\frac{3}{2}\sigma\phi\cos\theta_s\psi_a$$
$$-\frac{\partial\eta}{\partial\phi}\left(\nabla\mathbf{u}+\nabla\mathbf{u}^{\mathrm{T}}\right)\cdot\mathbf{u}_a\cdot\mathbf{n}+\omega_2\frac{\partial B}{\partial\phi}=0,\quad\text{on }\Gamma_{wall}, \tag{A.9d}$$

$$-\lambda\nabla\psi_a\cdot\mathbf{n}+(\mathbf{u}\cdot\mathbf{n})\phi_a-H(\varphi)\psi\mathbf{u}_a\cdot\mathbf{n}+\omega_1\frac{\partial A}{\partial\nabla\phi}\cdot\mathbf{n}+\omega_2\frac{\partial B}{\partial\phi}=0,\quad\text{on }\Gamma_{out}, \tag{A.9e}$$

$$M\nabla\phi_a\cdot\mathbf{n}+\omega_1\frac{\partial A}{\partial\nabla\psi}\cdot\mathbf{n}+\omega_2\frac{\partial B}{\partial\psi}=0,\quad\text{on }\partial\Omega, \tag{A.9f}$$

$$\phi_a(t=T)=-\frac{\partial\rho}{\partial\phi}\mathbf{u}\cdot\mathbf{u}_a,\quad\text{in }\Omega. \tag{A.9g}$$

Then, the adjoint sensitivity of the optimization problem in the optimization domain Ω is derived as

$$\delta\hat{J}(\Omega)$$
$$=\int_0^T\int_\Omega\left\{\omega_1\frac{\partial A}{\partial H(\varphi)}-\psi\nabla\phi\cdot\mathbf{u}_a+\rho\left(\alpha_f-\alpha_s\right)\mathbf{u}\cdot\mathbf{u}_a+\left(M_f-M_s\right)\nabla\psi\cdot\nabla\phi_a\right.$$

https://doi.org/10.4208/cicp.OA-2017-0003 Published online by Cambridge University Press

$$-\left(\lambda_f-\lambda_s\right)\nabla\phi\cdot\nabla\psi_a-\left(\lambda_f-\lambda_s\right)\frac{1}{\epsilon^2}\phi\left(\phi^2-1\right)\psi_a-\nabla\left[\frac{3}{4}\sigma_0\left(1-\phi^2\right)\cos\theta_s\psi_a+\omega_3 C\right]\cdot\mathbf{n}_\varphi$$
$$-\left[\frac{3}{4}\sigma_0\left(1-\phi^2\right)\cos\theta_s\psi_a+\omega_3 C\right]\kappa\Bigg\}\tau(\varphi)\delta\varphi\,\mathrm{d}\Omega\mathrm{d}t+\int_\Omega-\xi\tau(\varphi)\delta\varphi\,\mathrm{d}\Omega, \tag{A.10}$$

where $\mathbf{n}_\varphi=\frac{\nabla\varphi}{|\nabla\varphi|}$ and $\kappa=\nabla\cdot\mathbf{n}_\varphi$ are the unit normal vector and mean curvature of the level set function, respectively. In the optimization domain Ω, $\delta\hat{J}$ should satisfy $\delta\hat{J}>0$ for maximizing J, then $\mathbf{v}$, v_n and b can respectively be chosen to be

$$\mathbf{v}=\int_0^T\nabla\left[\frac{3}{4}\sigma_0\left(1-\phi^2\right)\cos\theta_s\psi_a+\omega_3 C\right]\mathrm{d}t, \tag{A.11a}$$
$$v_n=-\int_0^T\omega_1\frac{\partial A}{\partial H(\varphi)}-\psi\nabla\phi\cdot\mathbf{u}_a+\rho\left(\alpha_f-\alpha_s\right)\mathbf{u}\cdot\mathbf{u}_a+\left(M_f-M_s\right)\nabla\psi\cdot\nabla\phi_a$$
$$-\left(\lambda_f-\lambda_s\right)\nabla\phi\cdot\nabla\psi_a-\left(\lambda_f-\lambda_s\right)\frac{1}{\epsilon^2}\phi\left(\phi^2-1\right)\psi_a\mathrm{d}t+\xi, \tag{A.11b}$$
$$b=-\int_0^T\frac{3}{4}\sigma_0\left(1-\phi^2\right)\cos\theta_s\psi_a+\omega_3 C\,\mathrm{d}t. \tag{A.11c}$$

For minimizing J, $\delta\hat{J}$ should satisfy $\delta\hat{J}<0$, then the sign of $\mathbf{v}$, v_n and b in Eq. (A.11) is reversed. With the evolving velocity vector, normal evolving velocity and mean curvature evolving velocity obtained as Eq. (A.11) or its reverse, the level set function can be evolved to maximize or minimize the objective of the topology optimization problem in Eq. (3.1).

Acknowledgments

This work is supported by the National Natural Science Foundation of China (No. 51405465), the National High Technology Program of China (No. 2015AA042604), and Science and Technology Development Plan of Jilin Province and Changchun City (Nos. 20140201011GX, 15SS12, 20170312027ZG). The author is also grateful to the reviewers' kind attention and valuable suggestions.

References

[1] G. P. Steven, Q. Li and Y. M. Xie, Evolutionary topology and shape design for physical field problems, Comput. Mech., 26 (2000), 129-139.
[2] T. Borrvall and J. Petersson, Topology optimization of fluid in Stokes flow, Int. J. Numer. Meth. Fluids, 41 (2003), 77-107.
[3] M. P. Bendsoe and N. Kikuchi, Generating optimal topologies in optimal design using a homogenization method, Comput. Methods Appl. Mech. Engrg., 71 (1988), 197-224.
[4] O. Sigmund, A 99-line topology optimization code written in Matlab, Struct. Multidisc. Optim., 21 (2001), 120-127.

https://doi.org/10.4208/cicp.OA-2017-0003 Published online by Cambridge University Press

[5] O. Sigmund, On the design of compliant mechanisms using topology optimization, Mech. Struct. Mach., 25 (1997), 495-526.
[6] A. Saxena, Topology design of large displacement compliant mechanisms with multiple materials and multiple output ports, Struct. Multidisc. Optim., 30 (2005), 477-490.
[7] M. Bendsoe and O. Sigmund, Topology Optimization-Theory Methods and Applications, Springer, 2003.
[8] A. Gersborg-Hansen, M. P. Bendsoe and O. Sigmund, Topology optimization of heat conduction problems using the finite volume method, Struct. Multidisc. Optim., 31 (2006), 251-259.
[9] T. Nomura, K. Sato, K. Taguchi, T. Kashiwa and S. Nishiwaki, Structural topology optimization for the design of broadband dielectric resonator antennas using the finite difference time domain technique, Int. J. Numer. Methods Eng., 71 (2007), 1261-1296.
[10] O. Sigmund and K. G. Hougaard, Geometric properties of optimal photonic crystals, Phys. Rev. Lett., 100 (2008), 153904.
[11] M. B. Duhring, J. S. Jensen and O. Sigmund, Acoustic design by topology optimization, J. Sound Vibr., 317 (2008), 557-575.
[12] W. Akl, A. El-Sabbagh, K. Al-Mitani and A. Baz, Topology optimization of a plate coupled with acoustic cavity, Int. J. Solids Struct., 46 (2008), 2060-2074.
[13] Y. M. Xie and G. P. Steven, Evolutionary structural optimization, Springer, 1997.
[14] P. Tanskanen, The evolutionary structural optimization method: theoretical aspects, Comput. Methods Appl. Mech. Engrg., 191 (2002), 47-48.
[15] G. Allaire, Shape Optimization by the Homogenization Method, Springer-Verlag, New York, 2002.
[16] G. I. N. Rozvany, Aims scope methods history and unified terminology of computer-aided optimization in structural mechanics, Struct. Multidisc. Optim., 21 (2001), 90-108.
[17] M. P. Bendsoe and O. Sigmund, Material interpolations in topology optimization, Arch. Appl. Mech., 69 (1999), 635-654.
[18] J. K. Guest and J. H. Prevost, Topology optimization of creeping fluid flows using a Darcy-Stokes finite element, Int. J. Numer. Methods Eng., 66 (2006), 461-484.
[19] A. Gersborg-Hansen, O. Sigmund and R. B. Haber, Topology optimization of channel flow problems, Struct. Multidisc. Optim., 30 (2005), 181-192.
[20] M. Y. Wang, X. Wang and D. Guo, A level set method for structural optimization, Comput. Methods Appl. Mech. Engrg., 192 (2003), 227-246.
[21] G. Allaire, F. Jouve and A. Toader, Structural optimization using sensitivity analysis and a level-set method, J. Comput. Phys., 194 (2004), 363-393.
[22] S. Zhou and Q. Li, A variational level set method for the topology optimization of steady-state Navier-Stokes flow, J. Comput. Phys., 227 (2008), 10178-10195.
[23] X. Duan, Y. Ma and R. Zhang, Shape-topology optimization for Navier-Stokes problem using variational level set method, J. Comput. Appl. Math., 222 (2008), 487-499.
[24] Z. Liu and J. G. Korvink, Adaptive moving mesh level set method for structure optimization, Engrg. Optim., 40 (2008), 529-558.
[25] X. Xing, P. Wei and M. Y. Wang, A finite element-based level set method for structural optimization, Int. J. Numer. Methods Engrg., 82 (2010), 805-842.
[26] S. Kreissl, G. Pingen and K. Maute, An explicit level-set approach for generalized shape optimization of fluids with the lattice Boltzmann method, Int. J. Numer. Meth. Fluids, 65 (2011), 496-519.
[27] B. Bourdin and A. Chambolle, Optimisation topologique de structures soumises à des forces de pression, Actes du 32ème Congrès National d'Analyse Numérique, SMAI (ed.), 2000.

https://doi.org/10.4208/cicp.OA-2017-0003 Published online by Cambridge University Press

[28] B. Bourdin and A. Chambolle, Design-dependent loads in topology optimization, ESAIM: Control, Optimisation and Calculus of Variations, 9 (2003), 19-48.
[29] M. Burger and R. Stainko, Phase-field relaxation of topology optimization with local stress constraints, SIAM J. Control Optim., 45 (2006), 1447-1466.
[30] L. Blank, H. Garcke, L. Sarbu, T. Srisupattarawanit, V. Styles and A. Voig, Phase-field approaches to structural topology optimization, International Series of Numerical Mathematics, 160 (2012), 245-256.
[31] A. L. Gain and G. H. Paulino, Phase-field based topology optimization with polygonal elements: a finite volume approach for the evolution equation, Struct. Multidisc. Optim., 46 (2012), 327-342.
[32] S. Zhou and M. Y. Wang, Multimaterial structural topology optimization with a generalized CahnCHilliard model of multiphase transition, Struct. Multidisc. Optim., 33 (2007), 89-111.
[33] J. Liu, L. Dedè, J. A. Evans, M. J. Borden and T. J. R. Hughes, Isogeometric analysis of the advective Cahn-Hilliard equation: Spinodal decomposition under shear flow, J. Comput. Phys., 242 (2013), 321-350.
[34] A. Takezawa, S. Nishiwaki and M. Kitamura, Shape and topology optimization based on the phase field method and sensitivity analysis, J. Comput. Phys., 229 (2010), 2697-2718.
[35] Y. Deng, Z. Liu and Y. Wu, Optimization of unsteady incompressible Navier-Stokes flows using variational level set method, Int. J. Numer. Meth. Fluids, 71 (2013), 1475-1493.
[36] Y. Deng, Z. Liu and Y. Wu, Topology optimization of steady and unsteady incompressible Navier-Stokes flows driven by body forces, Struct. Multidisc. Optim., 47 (2013), 555-570.
[37] L. H. Olesen, F. Okkels and H. Bruus, A high-level programming-language implementation of topology optimization applied to steady-state Navier-Stokes flow, Int. J. Numer. Methods Eng., 65 (2006), 975-1001.
[38] Y. Deng, Z. Liu, P. Zhang, Y. Liu and Y. Wu, Topology optimization of unsteady incompressible Navier-Stokes flow, J. Comput. Phys., 230 (2011), 6688-6708.
[39] D. Makhija, G. Pingen, R. Yang and K. Maute, Topology optimization of multi-component flows using a multi-relaxation time lattice Boltzmann method, Comput. Fluids, 67 (2012), 104-114.
[40] J. Alexandersen, N. Aage, C. S. Andreasen and O. Sigmund, Topology optimisation for natural convection problems, Int. J. Numer. Meth. Fluids, 76 (2014), 699-721.
[41] M. S. Victor, G. V. Manuel and J. R. Clayton, Wetting and spreading dynamics, CRC Press, 2007.
[42] D. Gueyffier, J. Li, A. Nadim, R. Scardovelli and S. Zaleski, Volume-of-fluid interface tracking with smoothed surface stress methods for three-dimensional flows, J. Comput. Phys., 152 (1999), 423-456.
[43] J. Glimm, J. W. Grove, X. L. Li, K. M. Shyue, Q. Zhang and Y. Zeng, Three-dimensional front tracking, SIAM J. Sci. Comput., 19 (1998), 703-727.
[44] C. S. Peskin and D. M. McQueen, Modeling prosthetic heart valves for numerical analysis of blood flow in the heart, J. Comput. Phys., 37 (1980), 113-132.
[45] C. S. Peskin, The immersed boundary method, Acta Num., 11 (2002), 1-39.
[46] Y. C. Chang, T. Y. Hou, B. Merriman and S. Osher, A level set formulation of Eulerian interface capturing methods for incompressible fluid flows, J. Comput. Phys., 124 (1996), 449-464.
[47] M. Arienti and M. Sussman, An embedded level set method for sharp-interface multiphase simulations of Diesel injectors, Int. J. Multiphas. Flow, 59 (2014), 1-14.
[48] R. F. Engberga and E. Y. Kenig, An investigation of the influence of initial deformation on fluid dynamics of toluene droplets in water, Int. J. Multiphas. Flow, 76 (2015), 144-157.

https://doi.org/10.4208/cicp.OA-2017-0003 Published online by Cambridge University Press

[49] S. Osher and R. P. Fedkiw, Level set methods and dynamic implicit surfaces, Springer-Verlag, New York, 2002.
[50] J. A. Sethian and P. Smereka, Level set methods for fluid interfaces, Annu. Rev. Fluid Mech., 35 (2003), 341-372.
[51] H. A. A. Amiri and A. A. Hamouda, Evaluation of level set and phase field methods in modeling two phase flow with viscosity contrast through dual-permeability porous medium, Int. J. Multiphas. Flow, 52 (2013), 22-34.
[52] D. M. Anderson, G. B. McFadden and A. A. Wheeler, Diffuse-interface methods in fluid mechanics, Annu. Rev. Fluid Mech., 30 (1998), 139-165.
[53] D. Jacqmin, Calculation of two-phase Navier-Stokes flows using phase-field modeling, J. Comput. Phys., 155 (1999), 96-127.
[54] J. S. Kim, A continuous surface tension force formulation for diffuse-interface models, J. Comput. Phys., 204 (2005), 784-804.
[55] T. Qian, X. P. Wang and P. Sheng, Molecular hydrodynamics of the moving contact line in two-phase immiscible flows, Comm. Comput. Phys., 1 (2006), 1-52.
[56] D. Jacqmin, Contact-line dynamics of a diffuse fluid interface, J. Fluid Mech., 402 (2000), 57-88.
[57] J. W. Cahn and J. Hilliard, Free energy of a nonuniform system: I. Interfacial free energy, J. Chem. Phys., 28 (1958), 258-267.
[58] J. A. Sethian, Level set methods and fast marching methods evolving interfaces in computational geometry, fluid mechanics, computer vision, and materials science, Cambridge University Press, 1999.
[59] http://www.comsol.com
[60] J. W. Cahn, On spinodal decomposition, Acta Metall., 9 (1961), 795-801.
[61] J. W. Cahn, Critical-point wetting, J. Chem. Phys., 66 (1977), 3667-3672.
[62] P. Yue, C. Zhou, J. J. Feng, C. F. Ollivier-Gooch and H. H. Hu, Phase-field simulations of interfacial dynamics in viscoelastic fluids using finite elements with adaptive meshing, J. Comput. Phys., 219 (2006), 47-67.
[63] P. Yue, J. J. Feng, C. Liu and J. Shen, A diffuse-interface method for simulating two-phase flows of complex fluids, J. Fluid Mech., 515 (2004), 293-317.
[64] J. Nocedal and S. Wright, Numerical optimization, 2nd edition, Springer, 2000.
[65] H. C. Elman, D. J. Silvester and A. J. Wathen, Finite Elements and Fast Iterative Solvers: With Applications in Incompressible Fluid Dynamics, Oxford University Press, 2006.
[66] S. Osher and R. Fedkiw, Level Set Methods and Dynamic Implicit Surfaces, Springer-Verlag, New York, 2003.
[67] M. B. Giles, N. A. Pierce, An introduction to the adjoint approach to design, Flow Turbul. Combust., 65 (2000), 393-415.
[68] M. Hinze, R. Pinnau, M. Ulbrich and S. Ulbrich, Optimization with PDE Constraints, Springer: Berlin, 2009.
[69] B. Mohammadi and O. Pironneau, Applied Shape Optimization for Fluids, Oxford University Press, USA: Oxford, 2010.
[70] R. Defay and I. Prigogine, Surface Tension and Adsorption, Longmans, Green & Co Ltd, London, 1966.
[71] L. D. Landau and E. M. Lifshitz, Fluid Mechanics, Pergamon Press, Oxford, 1987.

https://doi.org/10.4208/cicp.OA-2017-0003 Published online by Cambridge University Press